Performance, results, and prospects of the visible spectrograph VEGA on CHARA

Denis Mourard[a], Mounir Challouf[a], Roxanne Ligi[a], Philippe Bério[a], Jean-Michel Clausse[a], Jérôme Gerakis[a], Laurent Bourges[b], Nicolas Nardetto[a], Karine Perraut[b], Isabelle Tallon-Bosc[c], H. McAlister[d,e], T. ten Brummelaar[e], S. Ridgway[f], J. Sturmann[e], L. Sturmann[e], N. Turner[e], C. Farrington[e] and P.J. Goldfinger[e]

[a]Laboratoire Lagrange, UMR 7293 UNS-CNRS-OCA, Boulevard de l'Observatoire, B.P. 4229, 06304 NICE Cedex 4, France.
[b]UJF-Grenoble 1 / CNRS-INSU, Institut de Planétologie et d'Astrophysique de Grenoble (IPAG) UMR 5274, Grenoble, F-38041, France.
[c]Université Lyon 1, Observatoire de Lyon, CNRS UMR5574, Ecole Normale Supérieure Lyon, 9 avenue Charles André, Saint-Genis Laval, F-69230, France
[d]Georgia State University, P.O. Box 3969, Atlanta GA 30302-3969, USA.
[e]CHARA Array, Mount Wilson Observatory, 91023 Mount Wilson CA, USA.
[f]National Optical Astronomy Observatory, PO Box 26732, Tucson, AZ 85726, USA

ABSTRACT

In this paper, we review the current performance of the VEGA/CHARA visible spectrograph and make a review of the most recent astrophysical results. The science programs take benefit of the exceptional angular resolution, the unique spectral resolution and one of the main features of CHARA: Infrared and Visible parallel operation. We also discuss recent developments concerning the tools for the preparation of observations and important features of the data reduction software. A short discussion of the future developments will complete the presentation, directed towards new detectors and possible new beam combination scheme for improved sensitivity and imaging capabilities.

Keywords: VEGA/CHARA, optical interferometry, visible wavelengths, data reduction software

1. INTRODUCTION

1.1 Main characteristics of CHARA and VEGA

The Center for High Angular resolution (CHARA) of the Georgia State University operates an optical interferometric array located at the Mount Wilson Observatory that consists of six one meter telescopes placed in pairs along the arms of a Y-shaped array. It yields 15 baselines ranging from 34 to 331 m. Operating in the near-infrared with CLASSIC[1] , CLIMB[2] , FLUOR[3] , and MIRC[4] , and in the visible with PAVO[5] and VEGA[6] , the CHARA array allows a maximum angular resolution of 1.3 and 0.3 millisecond of arc in the K and V band, respectively. The VEGA spectrograph is designed to sample the visible band from 0.45 to 0.85 μm with spectral resolutions of 1700, 5000, and up to 30000. It is equipped with two photon counting detectors that simultaneously study two different spectral bands at high and medium spectral resolution. The principle and performance of VEGA, in its two telescope mode, has been presented in Mourard et al., 2009[6] . Fringes with three and four telescopes[7] were obtained in 2010 .

The spectrograph is designed to sample the visible band from 0.45 to 0.85 μm. It is equipped with two photon counting detectors looking at two different spectral bands. The main characteristics are summarized in Tab. 1. The simultaneous operation of the two detectors is only possible in high and medium spectral resolution. The optical design allows simultaneous recording of data, in medium spectral resolution, of the spectral region around

---

$H\alpha$ with the red detector and around $H\beta$ with the blue detector. Observing in the blue requires good seeing conditions but increases by 30% the limit of spatial resolution of the instrument with respect to its operation around 700nm.

Grating	R	$\Delta\lambda$ (Blue)	$\Delta\lambda$ (Red)	$\lambda_R - \lambda_B$
R1: 1800gr/mm	30000	5 nm	8 nm	25 nm
R2: 300gr/mm	5000	30 nm	45 nm	170 nm
R3: 100gr/mm	1700	100 nm	150 nm	not possible

Table 1. Spectral resolution (R) and bandwidth ($\Delta\lambda$) of the VEGA spectrograph, as well as the spectral separation between the two detectors.

The limiting magnitudes of VEGA/CHARA are presented in Tab. 2. They of course highly depend on the actual seeing conditions and of the intrinsic target visibility.

Resolution	R	Typical Lim. Magnitude	Best perf.
Low	1700	6.8	7.5
Medium	6000	6.5	7.5
High	30000	4.2	5.5

Table 2. Estimation of typical limiting magnitude as a function of the different spectral resolution modes. These values are presented for the median value of r0 at Mount Wilson i.e. 8 cm. We also indicate the best performances assuming an r0 of 15 cm.

1.2 Summary of the current astrophysical programs

The VEGA instrument works in the visible domain [0.45μm;0.85μm] and benefits from three spectral resolutions, although the lowest one is no more used thanks to the difficulty of an accurate enough group delay tracking.

The medium (6000) and high (30000) spectral resolutions are well suited to perform kinematic analysis of the interferometric signal, providing resolution of 60 and 10km.s^{-1} respectively. These spectral resolutions are best dedicated to the extraction of differential spectral information. Radiative winds and fast rotating photospheres of hot stars can be probed efficiently with the medium spectral resolution. Some recent examples of such studies could be found for Be stars[8,9], interactive binaries,[10] young stellar objects[11] or the chromosphere of K giants[12].

The medium resolution is also well suited to absolute visibility studies and are also well adapted for the study of binaries or multiple systems. Recent results of such programs concern the study of roAp stars[13] or CoRoT targets[14] and more recently exoplanet hosts stars (Ligi et al. this conference).

Another interesting possibility is the presence of a polarimeter that could be inserted into the beam. This gives new insight into many physical processes. Many science sources are linearly polarized, in particular at a small angular scale, and the interferometric polarized signal is a powerful probe of circumstellar scattering environments that contain ionized gas or dust[15,16,17] and of magnetic properties[18,19].

1.3 Summary of the main known limitations

Despite the unique capabilities of VEGA/CHARA in terms of angular and spectral resolution, we have identified a certain number of limitations. The main one is the signal to noise ratio of the measurements at very low visibility and for the closure phase estimations. As it will be explained in Sect. 3.3, the reason is the multimode regime of the instrument induced by the short wavelength of operation and the diameter of the telescopes. The second main limitation comes from our photon-counting detectors presenting a saturation rate that prevents us to record individual frames with more than about 3000 photons. This means for example that for bright stars (magV<4 or 4.5 depending on the number of recombined telescopes) we need to use neutral densities. Thus the highly reduced signal to noise ratio causes high troubles for low visibility measurements.

2. INFORMATION FLOW IN VEGA OPERATIONS

2.1 General presentation

Preparing and scheduling optical interferometry observations requests specific steps based on different software tools. OCA (Observatoire de la Côte d'Azur) and JMMC have developed the PIVOT software (http://pivot-ws.oca.eu/) designed to help astronomers to prepare and schedule observations with the VEGA (Visible spEctro-Graph and polArimeter) instrument installed on the CHARA Array interferometer. It's based on a webservice compliant with virtual observatory technique using Axis2, Java, SAMP, XML and a MySql database. It allows different levels of functions from the deposit of proposals up to the direct night scheduling. This tool uses the interoperability capabilities with VO tools like SIMBAD or JMMC/ASPRO2 (see http://www.jmmc.fr/aspro_page.htm) all along the process.

PIVOT is divided in different phases: 1) Creation, management and modification of a proposal by each astronomer, 2) Management by the PI of run of all the proposals. Definition of the configurations with ASPRO2 and using a plugin aiming at calculating the pupil's positions, 3) Finalization of the proposal by the astronomer. Generation with ASPRO2 of the starlist file containing the list of observing blocks, edition of all the parameters, definition of the observing strategy and 4) Management of all the finalized proposals by the PI of the run/night and use of ASPRO2 for defining the detailed night schedule for each configuration.
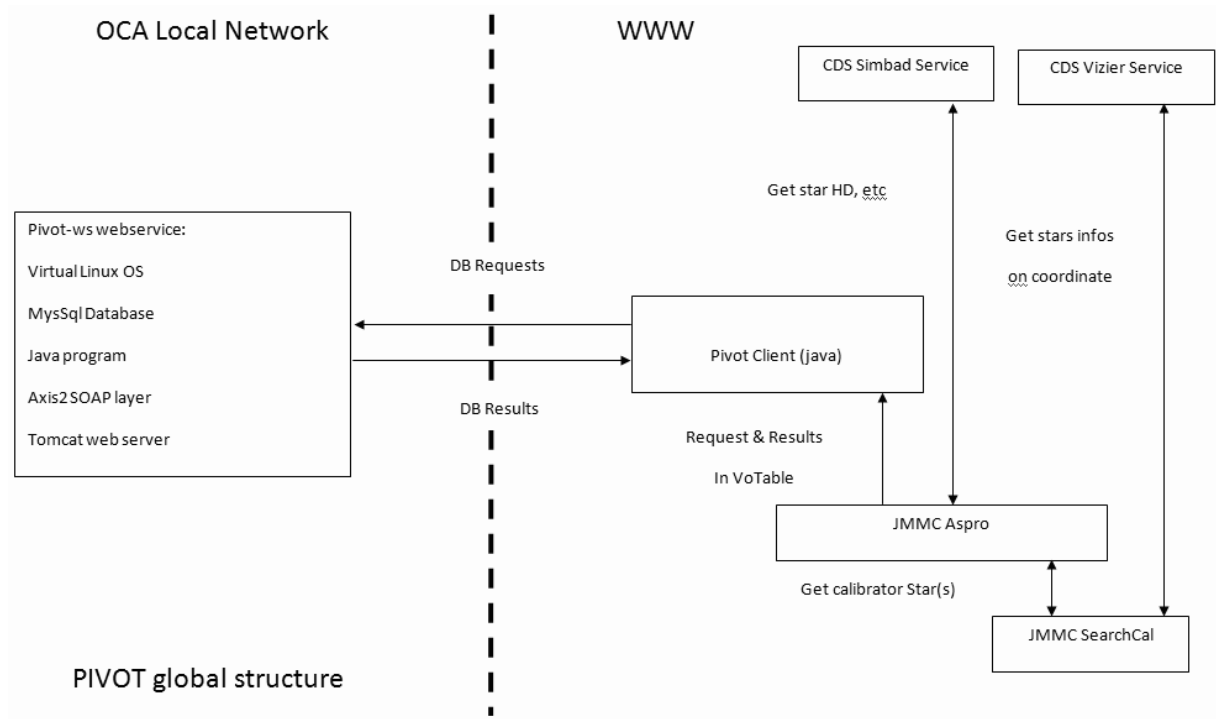

Figure 1. General architecture of the PIVOT database and of its interfaces.

In PIVOT we have defined actor's responsibility to protect the confidentiality and security of the data and also to define the behavior of software GUI (Graphical User Interface). Some widgets or notebook are displayed or hidden according to user status. The main classes are VEGA-PI, night- or run-PI, astronomer. The interoperability between PIVOT and ASPRO2 is based on the SAMP messaging protocol which uses VOTable format (XML) file for data exchange; both SAMP protocol and VOTable format are official Virtual Observatory (VO) standards provided by the International Virtual Observatory Alliance (IVOA http://ivoa.net/).

2.2 Software architecture

The webservice is installed on a virtual Linux operating system. We use the Axis2 package on a Tomcat server for the web interface. A Java program makes the link between the web server and the MySql database. This is
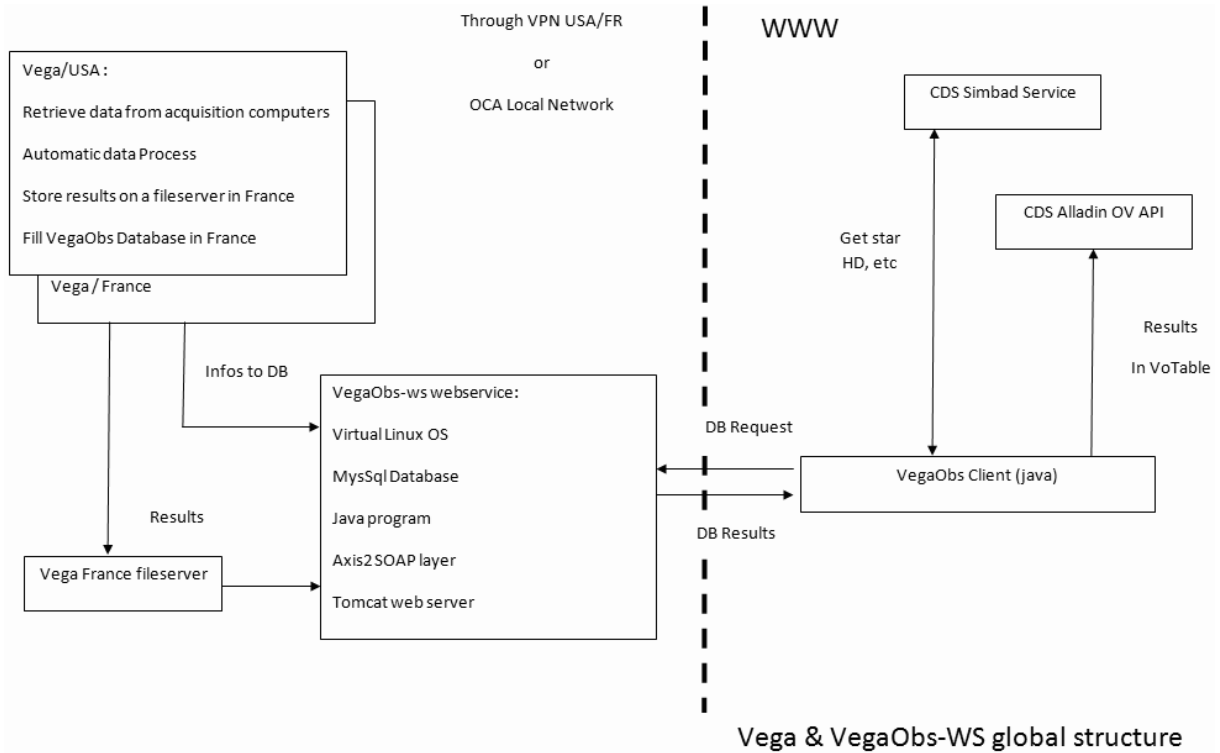
Figure 2. General architecture if the VEGAOBS database and of its interfaces.

a very basic and standalone system easy to install or reboot without any trouble to neighbor webservice on the same real computer. A graphical representation of this architecture is given in Fig. 1.

The Java software is developed on a personal computer with Netbeans which generate a ".war" file which only has to be put at the right place on the web server to be taken into account. We have developed for our own usage a Java client of our webservice then we are able to use it from everywhere in the world on a computer which have an up to date JVM (java virtual machine) installed.

2.3 Database structure

We have chosen a MySql database because we don't have a big amount of data or files to store. The database do not store the raw data but only the high level information regarding the observations. The database is divided in several tables to prevent information redundancy and to ease data management. MySql is also well supported by Java. We also built a second database aiming at storing all the information about actual observations. This second database (see Fig. 2, http://vegaobs-ws.oca.eu/) is automatically filled at the end of each night using an automatic script written in Python and using the log files of the night.

3. IMPROVEMENTS OF THE DATA REDUCTION PIPELINE

3.1 Transfer function analysis on a night basis

The aim of this subsection is to present the software tool that we have developed in order to obtain an estimation of the transfer function during one night of observation with VEGA/CHARA interferometer. This tool is very useful to explain how the *raw* squared visibilities obtained for one science target are calibrated in practical. As an example, we consider the following night: September, 1, 2011. The sequence of observation in the night is C1-S1-C2-S2-C3-S3-C3-C4-S4-C4-C5-S5-C5-S5. The "S" letters correspond to the observation of a science target, while C is for the observation of a calibrator for which we have an estimation of the angular diameter. For this night, we thus have : S1=10 Aql, S2=γ Lyr, S3=13 Cyg, C1= HD170878 ($\theta_{\mathrm{UD[V]}} = 0.239 \pm 0.017$mas),

C2= HD178233 ($\theta_{\mathrm{UD[V]}}$ = 0.393 ± 0.029mas), C3= HD177003 ($\theta_{\mathrm{UD[V]}}$ = 0.129 ± 0.009mas), C4= HD10205 ($\theta_{\mathrm{UD[V]}}$ = 0.225 ± 0.016mas), C5= HD26912 ($\theta_{\mathrm{UD[V]}}$ = 0.325 ± 0.023mas).

The sequence of observation is shown in Fig. 3.1 for the two different wavelength bandwidths: 705-725nm (upper panel), 725-745 (middle panel). The CHARA estimation of the Fried parameter r_0 is presented as a function of time in the lower panel. The *blue light* dots show the transfer function (T) calculated from the observations on the reference stars (C1 to C5) using the following formulae: $T^2 = \frac{\mu_{cal}^2}{V_{cal}^2}$, where μ_{cal} is the measured squared visibility on a given calibrator, while V_{cal}^2 is the expected squared visibility on the calibrator. For this night, we have a transfer function of typically 0.2. Each dot corresponds actually to one VEGA block (1000 images with exposure time of about 30 ms). An observation is composed of about 20-30 blocks (i.e. typically 10-15 mins; the user can define the number of blocks to reach the required Signal to Noise Ratio which depends also of the quality of the night). The horizontal lines superimposed over one observation is the corresponding *average* value calculated over the 20 or 30 blocks. The next step is to calibrate the *raw* squared visibilities measured for our science targets (defined as μ_{target}^2 and in *red dots* in the figure). For that, we consider an interpolation between the two calibrators next to the science observation and derive the final calibrated visibility using $V_{target}^2 = \frac{\mu_{target}^2}{T_{\mathrm{interpolated}}^2}$ (*yellow dots*). An interpolation has been done to calibrate S1, S2, and S3 (see dashed line). For S5, only one calibrator has been used, C5 (just before in time). In this case, there is no interpolation, only a simple division.
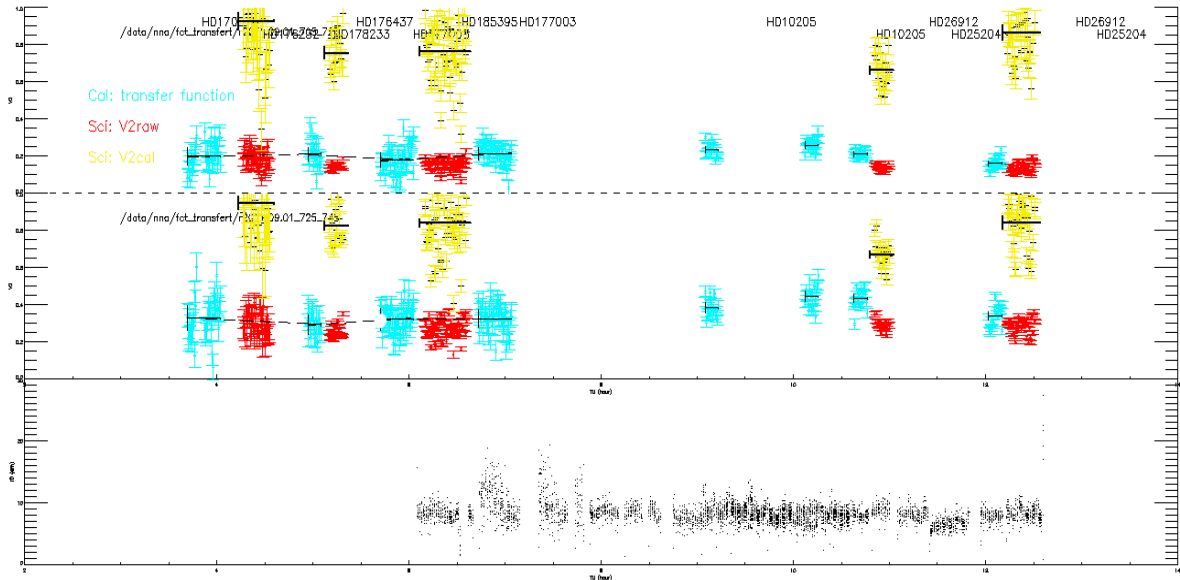

Figure 3. The time-sequences of *raw* science observations (red dots) are calibrated (yellow dots) using the transfer function (light blue dots). The transfer function is derived by comparing the observed and expected visibilities on reference stars. The bottom panel presents the evolution of the Fried parameter r_0 estimated through the tip/tilt information.

This kind of transfer function analysis is useful to test the consistency of the reference stars, and to define a good strategy of calibration. In the example that has been presented, we can consider that the night is stable enough to have confidence in the calibration process and to reduce the possible calibration bias to a level lower than the statistical accuracy of the measurements. Moreover, the seeing information is also a good indicator of the stability of the night.

3.2 Estimation of the error on the calibrated squared visibilities

As recalled in Sect 3.1, the calibration of the V^2 measurements on a *target* (or science object) is based on the temporally and spatially close observation of a star, the *calibrator* whose diameter is supposed to be known

with a given accuracy. The uncertainty on the knowledge of this *calibrator* contributes to the error on the final calibrated visibilities, but differently than the measurements themselves which lead to statistical errors. The purpose of this section is precisely to highlight analytically this distinction, which we take into account into the V^2 data processing.

3.2.1 Formalism of the V^2 estimation: depending of the measurements on the *calibrator*

The squared visibility of the target may be written as follows:

$$V_{target}^2 = V_{cal}^2 \; \frac{\mu_{target}^2}{\mu_{cal}^2}, \tag{1}$$

where V_{target}^2 and V_{cal}^2 are the true squared visibility of the target and the calibrator respectively, and μ_{target}^2 and μ_{cal}^2 their measured squared visibility. This equation assumes the constancy of the transfer function between the observations of the target and the calibrator.

The three terms of the right side of the equality are independent random variables. Whereas the product of two random variables, as $V_{cal}^2 \mu_{target}^2$, is calculable, the quotient of two random variables, here $V_{cal}^2 \mu_{target}^2$ by μ_{cal}^2, follows a law which does not have moments: neither the mean nor the variance is calculable and both must be estimated approximately. The approximation can be of a different order, depending on the value of the signal-to-noise ratio (SNR) of the denominator, i.e here on μ_{cal}^2. The SNR of a random variable is equal to the ratio of its mean on its standard deviation (or square root of its variance). To simplify the writing, we call α, β, γ the SNR of μ_{target}^2, μ_{cal}^2 and V_{cal}^2:

$$\alpha = \frac{< \mu_{target}^2 >}{\sigma_{\mu_{target}^2}}, \quad \beta = \frac{< \mu_{cal}^2 >}{\sigma_{\mu_{cal}^2}}, \quad \gamma = \frac{< V_{cal}^2 >}{\sigma_{V_{cal}^2}}, \tag{2}$$

$<>$ denoting the mean and σ the standard deviation. Using the study of Winzer[20] and the independence of the variables (cancelling covariance-terms), we found, **if β is larger than** 4, the following second order approximation with about 1% accuracy of both first moments of the quotient of Eq. 1:

$$< V_{target}^2 > \; \simeq \; < V_{cal}^2 >^2 \; \frac{< \mu_{target}^2 >^2}{< \mu_{cal}^2 >^2} \left[1 + \frac{1}{\beta^2} \right] \tag{3}$$

$$\sigma_{V_{target}^2}^2 \; \simeq \; < V_{target}^2 >^2 \left[\frac{1}{\alpha^2} + \frac{1}{\beta^2} + \frac{1}{\gamma^2} + \frac{1}{\beta^2 \gamma^2} - \frac{1}{\beta^4} \right] \tag{4}$$

Eq. 4 shows that the quadratic error on V_{target}^2 may be written as the sum of two terms, one of those being independent of γ, wich we call *statistic quadratic error*. The second term is named *systematic quadratic error*:

$$\sigma_{V_{target\,stat}^2}^2 \; \simeq \; < V_{cal}^2 >^2 \; \frac{< \mu_{target}^2 >^2}{< \mu_{cal}^2 >^2} \left[\frac{1}{\alpha^2} + \frac{1}{\beta^2} - \frac{1}{\beta^4} \right], \tag{5}$$

$$\sigma_{V_{target\,syst}^2}^2 \; \simeq \; < V_{cal}^2 >^2 \; \frac{< \mu_{target}^2 >^2}{< \mu_{cal}^2 >^2} \; \frac{1}{\gamma^2} \left[1 + \frac{1}{\beta^2} \right] \tag{6}$$

3.2.2 Influence of the true visibility of the *calibrator*

V_{cal}^2 is a statistical variable whose mean is the squared visibility related to the supposed geometrical shape of the calibrator. If this is a uniform disk of diameter θ_{UD}, the relation is:

$$< V_{cal}^2 > = 4 \left(\frac{J_1(z)}{z} \right)^2, \tag{7}$$

with $z = \pi < \theta_{UD} > B/\lambda$ where B is the baseline and λ the wavelength. $< \theta_{UD} >$ is given for example by SearchCal[21] after a polynomial fit in the (angular diameter, color indices) space with a standard deviation at one σ. We have numerically shown that, **if γ is larger than** 4, γ is proportional to the SNR of θ_{UD} as follows:

$$\frac{1}{\gamma} = 2z \left| \frac{J_2(z)}{J_1(z)} \right| \frac{\sigma \theta_{UD}}{< \theta_{UD} >}. \tag{8}$$

Eq. 7 and 8 are then inserted into the final equations of Section 3.2.1. We may verify that if the calibrator is well known, i.e. with a small uncertainty, $1/\gamma^2$ strongly decreases and the systematic quadratic error becomes negligible.

3.2.3 Extension of the formalism to the case of several *calibrator*s

An interferometric observation of a target classically needs the acquisition of a number n of calibrators sequences. They can be from the same calibrator but observed before and after the target, or from several different objects of reference. For estimating the calibrated V^2_{target}, we choose to consider the weighted mean of the estimators given by each calibrator individually, the weight beeing dependent on the statistic quadratic errors only:

$$< V^2_{target} > \quad \simeq \quad \frac{\sum_{i=1}^n w_i < V^2_{target} >_i}{\sum_{i=1}^n w_i}, \quad with \quad w_i = \frac{1}{\sigma^2_{V^2_{target\,stat_i}}}. \tag{9}$$

For the square standard deviation, taking care of always distinguish the systematic errors from the statistic ones yields a total quadratic error equal to the sum of both following terms:

$$\sigma^2_{V^2_{target\,stat}} \quad \simeq \quad \frac{1}{\sum_{i=1}^n w_i} \tag{10}$$

$$\sigma^2_{V^2_{target\,syst}} \quad \simeq \quad \frac{\sum_{i=1}^n \sigma^2_{V^2_{target\,syst_i}}}{n} \tag{11}$$

Eq. 9, 10 and 11 are inserted into the VEGA post-reduction tools. The latter warn the user of their limit of application: if β or γ is smaller than 4, the user is informed that the uncertainty on respectively, the measurements or the diameter of the calibrator, is not sufficient to be confident about the value of the calibrated squared visibility.

3.3 Error on the closure phase measurements

The problem of obtaining the most reliable estimate of the closure phase has been examined by a number of authors. Cornwell[22] showed that the closure phase is equal to the phase of the bispectrum (or triple product) and Woan & Duffett-Smith[23] showed that averaging the bispectrum is the best way to estimate the closure phase if the visibility phases cannot be recovered. The bispectrum is a complex valued function defined as:

$$D^{(3)}(u_1, v_1, u_2, v_2) = \tilde{I}(u_1, v_1)\tilde{I}(u_2, v_2)\tilde{I}^*(u_1 + u_2, v_1 + v_2) \tag{12}$$

where $\tilde{I}(\vec{u})$ is the Fourier transform of the fringe pattern and $\tilde{I}^*$ denotes the complex conjugate of $\tilde{I}$. The argument of the bispectrum is the closure phase $\Delta\phi$

$$\Delta\phi = arg[D^{(3)}(u_1, v_1, u_2, v_2)] = \theta_{12} + \theta_{23} - \theta_{13} \tag{13}$$

where θ_{ij} is visibility phase of baseline i j.

The error on the closure phase measurements is directly linked to the SNR of the bispectrum and more especially to SNR of the high frequency peak of the bispectrum corresponding to the triplet of baselines.

$$\sigma_{\Delta\phi} \approx \frac{1}{SNR_{BS}} \tag{14}$$

where SNR_{BS} represents the SNR of the high frequency peak of the bispectrum. Wirnitzer[24] gave the expression of the SNR of the bispectrum estimation in the case of observations in multi-speckle mode and with photon-counting detectors (see Eq. A13 in Wirnitzer (1985)). Fig. 3.3 shows the expected SNR of the high frequency peak of the bispectrum in the case of unresolved and resolved stars observed with VEGA. These curves have been computed assuming an exposure time of 15ms, a spectral bandwidth of 15nm centered at 700nm and 20000 frames. In Fig. 4, we notice that the SNR saturates for magnitudes below 4. This corresponds to the saturation limit of the VEGA photon-counting detectors. Actually, these detectors allow to record a maximum of 3600
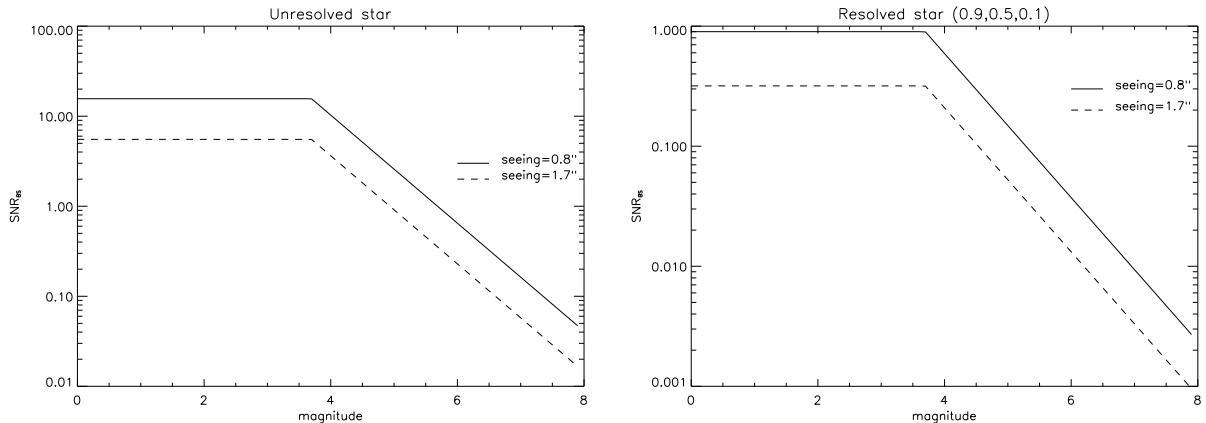
Figure 4. SNR of the high frequency peak of the bispectrum with respect to the star magnitude for an unresolved star (left) and a resolved star (right). The visibilities of the resolved star for the 3 baselines are 0.9, 0.5 and 0.1.

photons per frame only. For star brigther than magnitude 4, we observed usually with densities in order to operate below the detector limit.

Figure 4 illustrates perfectly the current limitation of VEGA in terms of closure phase measurements. Closure phase measurements for resolved star are very difficult (or almost impossible) whatever the star magnitude. An upgrade of the current photon-counting detector will be necessary for overcoming this limitation. A solution would be to reduce strongly the exposure time, up to 5ms (see Sec. 4). This will reject the SNR staturation limit to $m_V = 2$ allowing to measure closure phases for resolved stars with $2 < m_V < 4$ in case of good seeing conditions.

3.4 About the absolute orientation of the differential phases

Interference fringes contain both amplitude and phase information but atmospheric turbulence corrupts the observed fringe phases and various techniques must be used to recover this phase information: narrow-angle astrometry (a phase difference between two close objects is computed), differential phase (a phase difference between two different spectral channels (generally taken in the continuum and in a spectral line, respectively) is computed for a single object), and phase closure (a linear combination of phases between a triplet of telescopes is computed on a single object). Since VEGA is equipped with a spectrograph, differential phases (and visibilities) can be computed thanks to a cross-spectrum method.[6] These phases across a line give information about the photocenter position of the corresponding iso-velocity region: a differential phase signal (i.e. a fringe displacement) can be translated into a spatial displacement on the sky along the direction of the projected baseline. The absolute sign of the differential phase is thus of strong importance for kinematics studies.

In the CHARA focal lab, four beams denoted V1, V2, V3, and V4 can be allocated to VEGA that combines 2, 3, or 4 of them along the baselines 12, 23, 34, 13, 24, 14.

Each VEGA beam taken in the table BEAM=[V1, V2, V3, V4] can be fed by one telescope taken in the table TEL=[S1, S2, W1, W2, E2, E1] (in this order at the outputs of the delay lines - Fig. 5-left). Let us consider a baseline (Tel$_1$Tel$_2$) and denote T_{Tel_1} the rank of Tel$_1$, T_{Tel_2} the rank of Tel$_2$ in the TEL table, V_{Tel_1} the rank of Tel$_1$, and V_{Tel_2} the rank of Tel$_2$ in the BEAM table. Two beam configurations are possible: either $(T_{Tel_2} - T_{Tel_1}) * (V_{Tel_2} - V_{Tel_1}) < 0$ (Figure 5 up and right) or $(T_{Tel_2} - T_{Tel_1}) * (V_{Tel_2} - V_{Tel_1}) > 0$ (Figure 5 bottom and right) and the phase sign will be opposite for these two configurations.

In May 2010 we use technical time with average atmospheric conditions to calibrate the sign of the phase for the S2(V1)S1(V2) configuration with S1 as the reference (i.e. the delay line is on S2). We show that pointing an object towards the North tends to increase the interference order of the fringes. As a consequence a positive phase corresponds to an object towards S1 i.e. towards the South. This can be generalized for any Tel$_1$Tel$_2$ baseline .
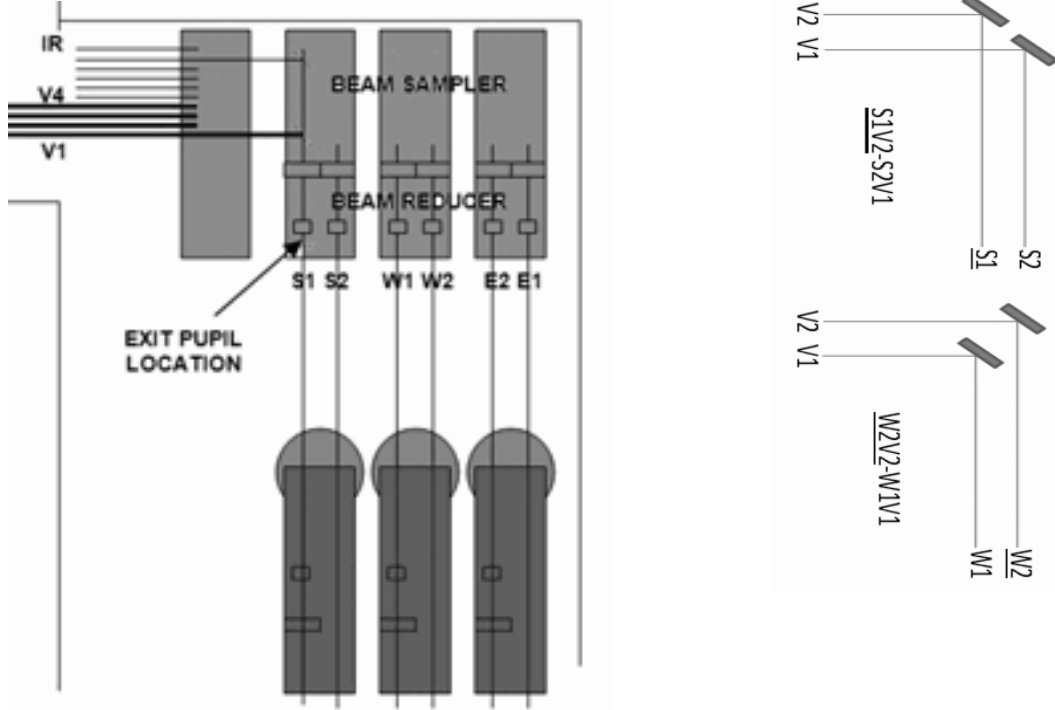
Figure 5. Left: Configuration of the CHARA beam switchyard presenting the ordering of delay line outputs and of the IR and Visible beams. Right: two opposite examples of possible beam configurations for feeding the VEGA/CHARA spectrograph.

- If $(T_{Tel_2} - T_{Tel_1}) * (V_{Tel_2} - V_{Tel_1}) < 0$, a positive phase signal corresponds to an object towards Tel_2.

- If $(T_{Tel_2} - T_{Tel_1}) * (V_{Tel_2} - V_{Tel_1}) > 0$, a positive phase signal corresponds to an object towards Tel_1.

The absolute orientation of the differential phase is now implemented routinely in the VEGA OIFITS file generation.

4. PROSPECTIVE

VEGA is in routine operation at Mount Wilson and benefits from about 60 nights per year. Many observations are now done remotely from Nice Observatory. Our group is currently working on the improvement of our photon counting detectors. A new image intensifier has been installed with better quantum efficiency (approximately a factor 1.5 better) in the red part of the spectrum and the Dalsa sensor[25] behind the two image intensifiers has been replaced by a Gazelle sensor from the Point Grey company. This new sensor will allow a faster frame rate (10ms) and a much lower dead time during two frames (1ms instead of 2ms. The duty cycle of the sensor will thus be of the order of 90% instead of the current 60%. We thus expect an improvement by a factor 2 or even more in case of bright star observations.

We are also considering a future evolution of VEGA in order to correctly benefit from the future installation of adaptive optics on the CHARA telescopes (T. ten Brummelaar, this conference). The high strehl ratio that will be allowed thanks to these new devices will concentrate the flux in a small part of the detector and thus will increase the saturation effect with the current generation of photon counting detector. We are now considering using analogical detector such as EMCCD or OCAM2 (P. Feautrier this conference) that allows a very high frame rate (up to 1500fps) and a very low readout noise ($0.13e^-/pix/frame$). Coupling this kind of detector with a beam combiner using spatial filtering and high efficiency optical devices (P. Bério in preparation) will permit to enhance the scientific domain of VEGA/CHARA in the future.

REFERENCES

[1] ten Brummelaar, T. A., McAlister, H. A., Ridgway, S. T., Bagnuolo, Jr., W. G., Turner, N. H., Sturmann, L., Sturmann, J., Berger, D. H., Ogden, C. E., Cadman, R., Hartkopf, W. I., Hopper, C. H., and Shure, M. A., "First Results from the CHARA Array. II. A Description of the Instrument," *ApJ* **628**, 453–465 (July 2005).

[2] Sturmann, J., Ten Brummelaar, T., Sturmann, L., and McAlister, H. A., "Dual three-way infrared beam combiner at the CHARA Array," in [*Proc. SPIE*], **7734** (July 2010).

[3] Coude du Foresto, V., Borde, P. J., Merand, A., Baudouin, C., Remond, A., Perrin, G. S., Ridgway, S. T., ten Brummelaar, T. A., and McAlister, H. A., "FLUOR fibered beam combiner at the CHARA array," in [*Society of Photo-Optical Instrumentation Engineers (SPIE) Conference Series*], Traub, W. A., ed., *Presented at the Society of Photo-Optical Instrumentation Engineers (SPIE) Conference* **4838**, 280–285 (Feb. 2003).

[4] Monnier, J. D., Zhao, M., Pedretti, E., Thureau, N., Ireland, M., Muirhead, P., Berger, J.-P., Millan-Gabet, R., Van Belle, G., ten Brummelaar, T., McAlister, H., Ridgway, S., Turner, N., Sturmann, L., Sturmann, J., Berger, D., Tannirkulam, A., and Blum, J., "Imaging the surface of Altair and a MIRC update," in [*Society of Photo-Optical Instrumentation Engineers (SPIE) Conference Series*], *Presented at the Society of Photo-Optical Instrumentation Engineers (SPIE) Conference* **7013** (July 2008).

[5] Ireland, M. J., Mérand, A., ten Brummelaar, T. A., Tuthill, P. G., Schaefer, G. H., Turner, N. H., Sturmann, J., Sturmann, L., and McAlister, H. A., "Sensitive visible interferometry with PAVO," in [*Society of Photo-Optical Instrumentation Engineers (SPIE) Conference Series*], *Presented at the Society of Photo-Optical Instrumentation Engineers (SPIE) Conference* **7013** (July 2008).

[6] Mourard, D., Clausse, J. M., Marcotto, A., Perraut, K., Tallon-Bosc, I., Bério, P., Blazit, A., Bonneau, D., Bosio, S., Bresson, Y., Chesneau, O., Delaa, O., Hénault, F., Hughes, Y., Lagarde, S., Merlin, G., Roussel, A., Spang, A., Stee, P., Tallon, M., Antonelli, P., Foy, R., Kervella, P., Petrov, R., Thiebaut, E., Vakili, F., McAlister, H., Ten Brummelaar, T., Sturmann, J., Sturmann, L., Turner, N., Farrington, C., and Goldfinger, P. J., "VEGA: Visible spEctroGraph and polArimeter for the CHARA array: principle and performance," *A&A* **508**, 1073–1083 (Dec. 2009).

[7] Mourard, D., Bério, P., Perraut, K., Ligi, R., Blazit, A., Clausse, J. M., Nardetto, N., Spang, A., Tallon-Bosc, I., Bonneau, D., Chesneau, O., Delaa, O., Millour, F., Stee, P., Le Bouquin, J. B., Ten Brummelaar, T., Farrington, C., Goldfinger, P. J., and Monnier, J. D., "Spatio-spectral encoding of fringes in optical long-baseline interferometry. Example of the 3T and 4T recombining mode of VEGA/CHARA," *A&A* **531**, A110 (July 2011).

[8] Delaa, O., Stee, P., Meilland, A., Zorec, J., Mourard, D., Bério, P., Bonneau, D., Chesneau, O., Clausse, J. M., Cruzalebes, P., Perraut, K., Marcotto, A., Roussel, A., Spang, A., McAlister, H., Ten Brummelaar, T., Sturmann, J., Sturmann, L., Turner, N., Farrington, C., and Goldfinger, P. J., "Kinematics and geometrical study of the Be stars 48 Persei and ψ Persei with the VEGA/CHARA interferometer," *A&A* **529**, A87 (May 2011).

[9] Meilland, A., Delaa, O., Stee, P., Kanaan, S., Millour, F., Mourard, D., Bonneau, D., Petrov, R., Nardetto, N., Marcotto, A., Roussel, A., Clausse, J. M., Perraut, K., McAlister, H., Ten Brummelaar, T., Sturmann, J., Sturmann, L., Turner, N., Ridgway, S. T., Farrington, C., and Goldfinger, P. J., "The binary Be star δ Scorpii at high spectral and spatial resolution. I. Disk geometry and kinematics before the 2011 periastron," *A&A* **532**, A80 (Aug. 2011).

[10] Bonneau, D., Chesneau, O., Mourard, D., Bério, P., Clausse, J. M., Delaa, O., Marcotto, A., Perraut, K., Roussel, A., Spang, A., Stee, P., Tallon-Bosc, I., McAlister, H., Ten Brummelaar, T., Sturmann, J., Sturmann, L., Turner, N., Farrington, C., and Goldfinger, P. J., "A large Hα line forming region for the massive interacting binaries β Lyrae and υ Sagitarii," *A&A* **532**, A148 (Aug. 2011).

[11] Rousselet-Perraut, K., Benisty, M., Mourard, D., Rajabi, S., Bacciotti, F., Bério, P., Bonneau, D., Chesneau, O., Clausse, J. M., Delaa, O., Marcotto, A., Roussel, A., Spang, A., Stee, P., Tallon-Bosc, I., McAlister, H., Ten Brummelaar, T., Sturmann, J., Sturmann, L., Turner, N., Farrington, C., and Goldfinger, P. J., "The Hα line forming region of AB Aurigae spatially resolved at sub-AU with the VEGA/CHARA spectro-interferometer," *A&A* **516**, L1 (June 2010).

[12] Berio, P., Merle, T., Thévenin, F., Bonneau, D., Mourard, D., Chesneau, O., Delaa, O., Ligi, R., Nardetto, N., Perraut, K., Pichon, B., Stee, P., Tallon-Bosc, I., Clausse, J. M., Spang, A., McAlister, H., Ten Brummelaar, T., Sturmann, J., Sturmann, L., Turner, N., Farrington, C., and Goldfinger, P. J., "Chromosphere of K giant stars. Geometrical extent and spatial structure detection," *A&A* **535**, A59 (Nov. 2011).

[13] Perraut, K., Brandão, I., Mourard, D., Cunha, M., Bério, P., Bonneau, D., Chesneau, O., Clausse, J. M., Delaa, O., Marcotto, A., Roussel, A., Spang, A., Stee, P., Tallon-Bosc, I., McAlister, H., Ten Brummelaar, T., Sturmann, J., Sturmann, L., Turner, N., Farrington, C., and Goldfinger, P. J., "The fundamental parameters of the roAp star γ Equulei," *A&A* **526**, A89 (Feb. 2011).

[14] Bigot, L., Mourard, D., Berio, P., Thévenin, F., Ligi, R., Tallon-Bosc, I., Chesneau, O., Delaa, O., Nardetto, N., Perraut, K., Stee, P., Boyajian, T., Morel, P., Pichon, B., Kervella, P., Schmider, F. X., McAlister, H., Ten Brummelaar, T., Ridgway, S. T., Sturmann, J., Sturmann, L., Turner, N., Farrington, C., and Goldfinger, P. J., "The diameter of the CoRoT target HD 49933. Combining the 3D limb darkening, asteroseismology, and interferometry," *A&A* **534**, L3 (Oct. 2011).

[15] Elias, II, N. M., Jones, C. E., Schmitt, H. R., Jorgensen, A. M., Ireland, M. J., and Perraut, K., "The case for optical interferometric polarimetry," *ArXiv e-prints* (Nov. 2008).

[16] Ireland, M. J., Tuthill, P. G., Davis, J., and Tango, W., "Dust scattering in the Miras R Car and RR Sco resolved by optical interferometric polarimetry," *MNRAS* **361**, 337–344 (July 2005).

[17] Chesneau, O., Wolf, S., and Domiciano de Souza, A., "Hot stars mass-loss studied with Spectro-Polarimetric INterferometry (SPIN)," *A&A* **410**, 375–388 (Oct. 2003).

[18] Rousselet-Perraut, K., Chesneau, O., Berio, P., and Vakili, F., "Spectro-polarimetric interferometry (SPIN) of magnetic stars," *A&A* **354**, 595–604 (Feb. 2000).

[19] Rousselet-Perraut, K., Stehlé, C., Lanz, T., Le Bouquin, J. B., Boudoyen, T., Kilbinger, M., Kochukhov, O., and Jankov, S., "Stellar activity and magnetism studied by optical interferometry," *A&A* **422**, 193–203 (July 2004).

[20] Winzer, P., "Accuracy of error propagation exemplified with ratios of random variables," *Rev. Sci. Instrum.* **71-3**, 1447–1454 (2000).

[21] Bonneau, D., Clausse, J.-M., Delfosse, X., Mourard, D., Cetre, S., Chelli, A., Cruzalèbes, P., Duvert, G., and Zins, G., "Searchcal: a virtual observatory tool for searching calibrators in optical long baseline interferometry. i. the bright object case," *Astron. Astrophys.* **456**, 789– (2006).

[22] Cornwell, T. J., "Radio-interferometric imaging of weak objects in conditions of poor phase stability - the relationship between speckle masking and phase closure methods," *A&A* **180**, 269–274 (June 1987).

[23] Woan, G. and Duffett-Smith, P. J., "Determination of Closure Phase in Noisy Conditions," *A&A* **198**, 375 (June 1988).

[24] Wirnitzer, B., "Bispectral analysis at low light levels and astronomical speckle masking," *Journal of the Optical Society of America A* **2**, 14–21 (Jan. 1985).

[25] Blazit, A., Rondeau, X., Thiébaut, E., Abe, L., Bernengo, J., Chevassut, J., Clausse, J., Dubois, J., Foy, R., Mourard, D., Patru, F., Spang, A., Tallon-Bosc, I., Tallon, M., Tourneur, Y., and Vakili, F., ""New generation photon-counting cameras: algol and CPNG."," *Applied Optics* **47**(8), 1141–1151 (2008).